

See discussions, stats, and author profiles for this publication at: <https://www.researchgate.net/publication/320659159>

# Intercomparison of attenuation correction algorithms for single-polarized X-band radars

Article in *Atmospheric Research* · October 2017

DOI: 10.1016/j.atmosres.2017.10.020

CITATIONS

0

READS

73

3 authors, including:



[Katharina Lengfeld](#)

Deutscher Wetterdienst

14 PUBLICATIONS 30 CITATIONS

[SEE PROFILE](#)



[Marc Berenguer](#)

Universitat Politècnica de Catalunya

80 PUBLICATIONS 752 CITATIONS

[SEE PROFILE](#)

Some of the authors of this publication are also working on these related projects:



Radar Technology [View project](#)



ANYWHERE - EnhANCing emergencY management and response to extreme WeatHER and climate Events - Horizon 2020 - Secure Societies [View project](#)



# Intercomparison of attenuation correction algorithms for single-polarized X-band radars



K. Lengfeld<sup>a,b,\*</sup>, M. Berenguer<sup>b</sup>, D. Sempere Torres<sup>b</sup>

<sup>a</sup> Deutscher Wetterdienst, Offenbach am Main, Germany

<sup>b</sup> Centre de Recerca Aplicada en Hidrometeorologia, Universitat Politècnica de Catalunya, Barcelona, Spain

## ARTICLE INFO

### Keywords:

X-band radar

Single-polarization

Attenuation correction

## ABSTRACT

Attenuation due to liquid water is one of the largest uncertainties in radar observations. The effects of attenuation are generally inversely proportional to the wavelength, i.e. observations from X-band radars are more affected by attenuation than those from C- or S-band systems. On the other hand, X-band radars can measure precipitation fields in higher temporal and spatial resolution and are more mobile and easier to install due to smaller antennas.

A first algorithm for attenuation correction in single-polarized systems was proposed by Hitschfeld and Bordan (1954) (*HB*), but it gets unstable in case of small errors (e.g. in the radar calibration) and strong attenuation. Therefore, methods have been developed that restrict attenuation correction to keep the algorithm stable, using e.g. surface echoes (for space-borne radars) and mountain returns (for ground radars) as a final value (*FV*), or adjustment of the radar constant (*C*) or the coefficient  $\alpha$ . In the absence of mountain returns, measurements from C- or S-band radars can be used to constrain the correction. All these methods are based on the statistical relation between reflectivity and specific attenuation. Another way to correct for attenuation in X-band radar observations is to use additional information from less attenuated radar systems, e.g. the ratio between X-band and C- or S-band radar measurements. Lengfeld et al. (2016) proposed such a method based isotonic regression of the ratio between X- and C-band radar observations along the radar beam.

This study presents a comparison of the original *HB* algorithm and three algorithms based on the statistical relation between reflectivity and specific attenuation as well as two methods implementing additional information of C-band radar measurements. Their performance in two precipitation events (one mainly convective and the other one stratiform) shows that a restriction of the *HB* is necessary to avoid instabilities. A comparison with vertically pointing micro rain radars (MRR) reveals good performance of two of the methods based in the statistical *k-Z*-relation: *FV* and  $\alpha$ . The *C* algorithm seems to be more sensitive to differences in calibration of the two systems and requires additional information from C- or S-band radars.

Furthermore, a study of five months of radar observations examines the long-term performance of each algorithm. From this study conclusions can be drawn that using additional information from less attenuated radar systems lead to best results. The two algorithms that use this additional information eliminate the bias caused by attenuation and preserve the agreement with MRR observations.

## 1. Introduction

Heavy and long-lasting precipitation is one of the largest natural hazards in Europe causing serious damage, especially in urban areas. In order to prevent damage and manage the risk of heavy precipitation, understanding and forecasting these events is crucial and requires detailed information on the high variability of precipitation in space and time. National and regional radar networks for rainfall observation typically consist of radar systems that operate in the C- or S-band

frequency range. These systems are designed to provide spatial information on precipitation for large areas with temporal resolution in the order of 5 min and spatial resolution in the order of a few 100 m. However, Ochoa-Rodriguez et al. (2015) studied the influence of temporal and spatial resolution on rainfall runoff simulations and advised a minimum of 5 min and  $\sim 0.1$  km for hydrological applications in urban areas with drainage areas smaller than 1 ha. Rafieeiniasab et al. (2015) also emphasize the importance of temporally high-resolution precipitation for flash flood forecasting in urban areas.

\* Corresponding author.

E-mail address: [katharina.lengfeld@dwd.de](mailto:katharina.lengfeld@dwd.de) (K. Lengfeld).

A promising addition to national radar networks are systems that operate at shorter wavelength, because the resolution depends, among other factors, on antenna size and wavelength. Furthermore, these systems are more mobile, easier to install and cost effective due to the smaller antenna size. Lengfeld et al. (2014) and Trabal et al. (2013) suggest that observations at X-band frequency meet present and future demands of resolution. A number of studies have shown that these high-resolution X-band weather radars can fill gaps in nationwide networks or be used for further investigating areas of special interest, e.g. mountainous regions (Beck and Bousquet, 2013; Figuras i Ventura, J., Tabary P., 2013; Shakti et al., 2013), urban areas (Berenguer et al., 2012; Chen and Chandrasekar, 2012; van de Beek, C. Z. et al., 2013), airports (Turso et al., 2009) and regions prone to floods (Matrosov et al., 2013).

A disadvantage of X-band radar systems is significant attenuation by liquid water (Atlas and Ulbrich, 1977; Gunn and East, 1954). The magnitude of attenuation is generally inversely proportional to the wavelength, i.e. observations from X-band radars are more affected by attenuation than those from C- and S-band systems. As proposed in many studies, measurements obtained from dual-polarization, e.g. differential phase, can be used to estimate attenuation (Bringi et al., 1990; Feng et al., 2016; Ryzhkov and Zrnic, 1995) but dual-polarized systems are currently much more expensive than single-polarized radars.

Hitschfeld and Bordan (1954) proposed the first algorithm for attenuation correction in single-polarized systems based on the statistical relation between measured reflectivity and specific attenuation. The downside of this method is its instability, especially for shorter wavelengths, in case of strong precipitation and, therefore, strong attenuation or errors in reflectivity measurements. To overcome this drawback for single-polarized X-band radars, fixed targets are used to constrain the Hitschfeld and Bordan algorithm. Meneghini et al. (1983) introduced a method including ground clutter returns for vertically pointing space-borne X-band radars, Delrieu et al. (1997) made use of mountain returns for scanning X-band radars. Iguchi and Meneghini (1994) investigated several single-frequency attenuation correction methods for airborne radars and proposed a hybrid method that combines the Hitschfeld and Bordan method, that performs well at low attenuations, with a surface reference method. In the absence of surface or mountain returns, data from less attenuated observations of the national C- or S-band radar network can be taken to restrict the attenuation correction (Berenguer et al., 2012). Similarly, Lengfeld et al. (2016) suggested an algorithm that is independent of the statistical relation between reflectivity and attenuation. They used the ratio between X- and C-band radar measurements not only at the end of each X-band radar beam but in the whole area covered by the X-band radar and calculated an attenuation correction factor for each bin along the beam using isotonic regression.

This paper presents a comparison of the original HB attenuation correction algorithm, four algorithms based on the k-Z-relation as proposed by Iguchi and Meneghini (1994) as well as the method by Lengfeld et al. (2016) using the ratio between X- and C-band radar measurements. It is structured as follows: An overview of the attenuation correction algorithms is given in Section 2. The X- and C-band radar systems are described in Section 3 as well as the investigated precipitation events. Section 4 contains results for two different case studies, a convective and a stratiform event. Furthermore, a study of 5 months of radar observations examines the longterm performance of each method. Conclusions are drawn in Section 5.

## 2. Attenuation correction algorithms

In this study, three different approaches for attenuation correction are applied to observations of a single-polarized non-Doppler X-band radar system. The first is the original attenuation correction algorithm proposed by Hitschfeld and Bordan (1954) (HB hereafter). It is based only on reflectivity measurements obtained by the X-band radar system.

**Table 1**

Overview of the investigated attenuation correction algorithms.

Name	Description	Use of C-band data
HB	Original algorithm as proposed by Hitschfeld and Bordan (1954)	No
FV	Uses total attenuation at the maximum range as restriction	Last range bin
$\alpha$	Based on the adjustment of $\alpha$	Last range bin
C	Based on the adjustment of the radar constant	Last range bin
$C_{\max}$	Based on the adjustment of the radar constant	First and last range bin
ISO	Isotonic regression of reflectivity ratio between C- and X-band radar along each beam	All range bins

The other two approaches make use of the assumption that C-band radars are less affected by path attenuation due to precipitation than X-band radars because of their larger wavelength: (i) an approach based on backward attenuation correction as proposed by Iguchi and Meneghini (1994), and (ii) an approach that directly uses the difference between X- and C-band reflectivities as proposed by Lengfeld et al. (2016). An overview of the algorithms investigated is given in Table 1.

In the following, we use the same notation as Iguchi and Meneghini (1994). The backscattered power from a range  $r$  [km] can be described as a function of the measured reflectivity factor  $Z_m$  [mm<sup>6</sup> m<sup>-3</sup>] along the path:

$$P(r) = \frac{CZ_m(r)}{r^2}. \quad (1)$$

$C$  is the radar constant and  $Z_m(r)$  is related to the non-attenuated reflectivity factor  $Z(r)$  through the two-way attenuation factor  $A(r)$ :

$$Z_m(r) = Z(r)A(r) \quad (2)$$

with

$$A(r) = \exp \left[ -0.2 \ln(10) \int_0^r k(s) ds \right]. \quad (3)$$

Assuming that the specific attenuation  $k(r)$  in dB km<sup>-1</sup> is related to  $Z(r)$  through a power law,  $k = \alpha Z^\beta$ , with wavelength dependent constants  $\alpha$  and  $\beta$ , Iguchi and Meneghini (1994) derived a general solution for Eq. (2):

$$Z(r) = Z_m(r)[C_1 - qS(r)]^{-1/\beta} \quad (4)$$

with a constant  $C_1$ ,  $q = 0.2\beta \ln(10)$  and

$$S(r) = \int_0^r \alpha Z_m^\beta(s) ds, \quad (5)$$

with  $\alpha$  and  $\beta$  for X-band radars according to Delrieu et al. (1997).

In the solution proposed by Hitschfeld and Bordan (1954),  $C_1 = 1$  due to the initial condition that  $Z(r) = Z_m(r)$  at the radar, where  $r = 0$ :

$$Z_{HB}(r) = Z_m(r)[1 - qS(r)]^{-1/\beta}. \quad (6)$$

A well-known problem of the HB algorithm is its instability with errors in  $Z_m$  in case of high reflectivities and, therefore, strong attenuation. A detailed study of the sensitivity and errors in attenuation correction for X-band radar measurements can be found in Berne and Uijlenhoet (2006). To overcome this disadvantage Iguchi and Meneghini (1994) proposed an extension of the HB method for space-borne radars by taking into account total attenuation at the maximum range of the radar, i.e. at the surface ( $r_s$ ):

$$C_1 = \left[ \frac{Z_m(r_s)}{Z(r_s)} \right]^\beta + qS(r_s). \quad (7)$$

However, the final value (FV) algorithm in this form only works for space-borne radars because it makes use of the surface echo. For the

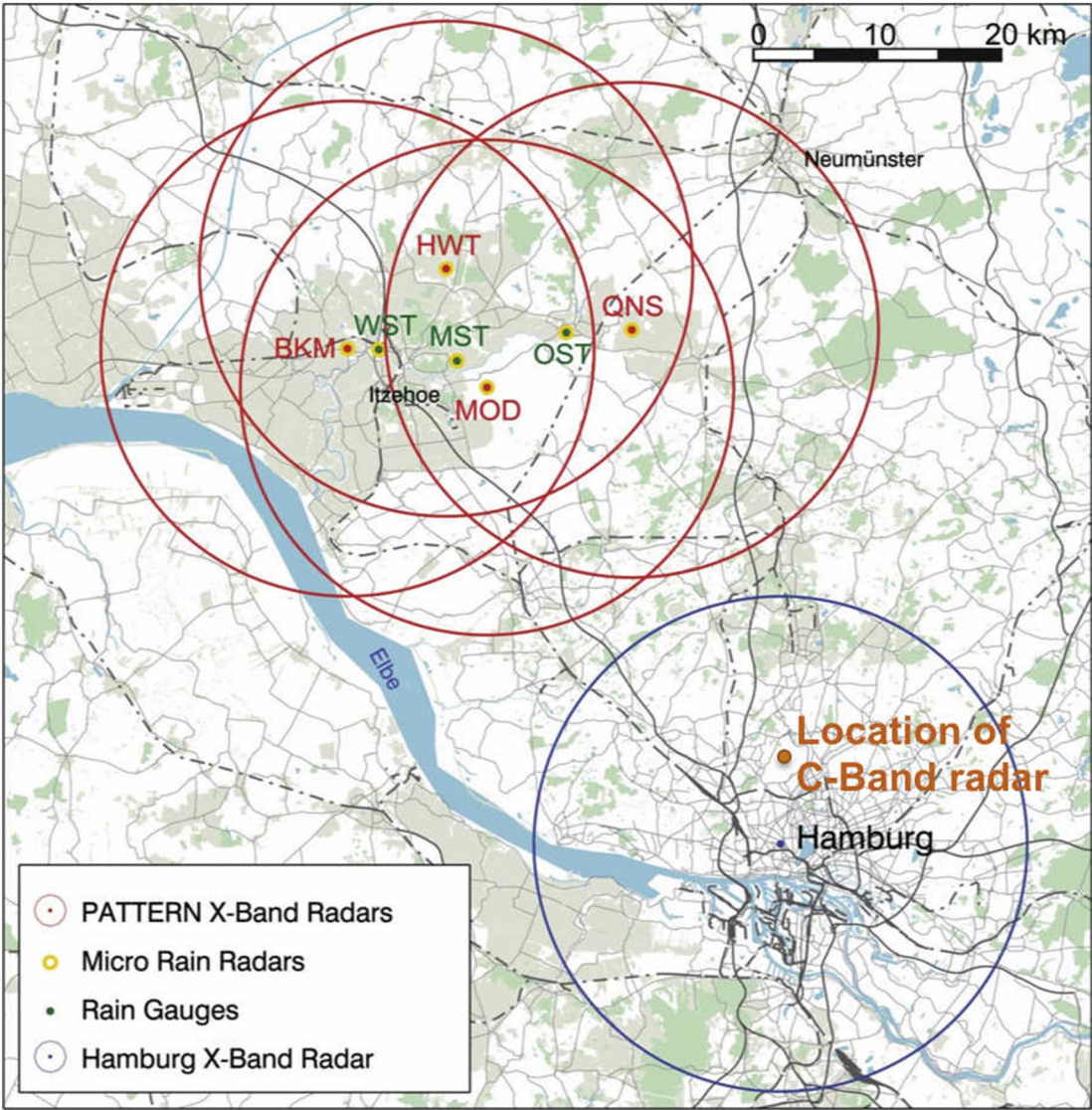


**Fig. 1.** Map of the 5 X-band radars and reference stations in Northern Germany. Positions and maximum ranges of the four network radars Hungriger Wolf Tower (HWT), Quarnstedt (QNS), Bekmünde (BKM) and Moordorf (MOD) are indicated by red dots and circles, respectively. The Hamburg X-band radar and its maximum range is indicated by the blue dot and circle. The orange dot marks the location of the C-band radar in the northern part of Hamburg. It has a maximum range of 128 km and covers the whole area. Rain gauges OST, MST and WST are marked by green dots. Micro rain radars are depicted as yellow circles. (For interpretation of the references to color in this figure legend, the reader is referred to the web version of this article.)

**Table 2**  
Specification of X-band LAWR and C-band radar products.

Parameters	X-band	C-band
Range resolution	60 m	1 km
Azimuth resolution	1°	1°
Time resolution	30 s	5 min
Maximum range	20 km	128 km
Calibration accuracy	± 1 dB	± 2 dB
Transmit power	25 kW	250 kW
Frequency	9410 MHz	5640 MHz
Pulse width	0.4 μs	0.8 μs
Pulse repetition frequency	800 Hz	600 Hz
Beam width	2.8°	1°

ground-based scanning X-band radar used in this study the estimate of total attenuation at the maximum range bin filled with rain ( $r_{max}$ ) is obtained by comparison with a less attenuated C-band radar that overlaps with the X-band radar leading to the following estimation of Z:

$$Z_{FV}(r) = Z_m(r)[A(r_{max})^\beta + q[S(r_{max}) - S(r)]^{-1/\beta}]^{-1/\beta}, \tag{8}$$

with

$$A(r_{max}) = \frac{Z_m(r_{max})}{Z_{Cband}(r_{max})}. \tag{9}$$

and  $Z_{Cband}$  is the reflectivity measured by the C-band radar.

Iguchi and Meneghini (1994) also suggested two other solutions that adjust the coefficient  $\alpha$  and the radar constant  $C$ , called the  $\alpha$ - and the  $C$ -method hereafter:

$$Z_\alpha(r) = Z_m(r)[1 - \epsilon qS(r)]^{-1/\beta} \tag{10}$$

$$Z_C(r) = Z_m(r)\epsilon^{1/\beta}[1 - qS(r)]^{-1/\beta}, \tag{11}$$

where

$$\epsilon = \frac{1 - A(r_{max})^\beta}{qS(r_{max})}. \tag{12}$$

A detailed description and analysis of the  $FV$ ,  $\alpha$  and  $C$  methods can be found in Iguchi and Meneghini (1994).

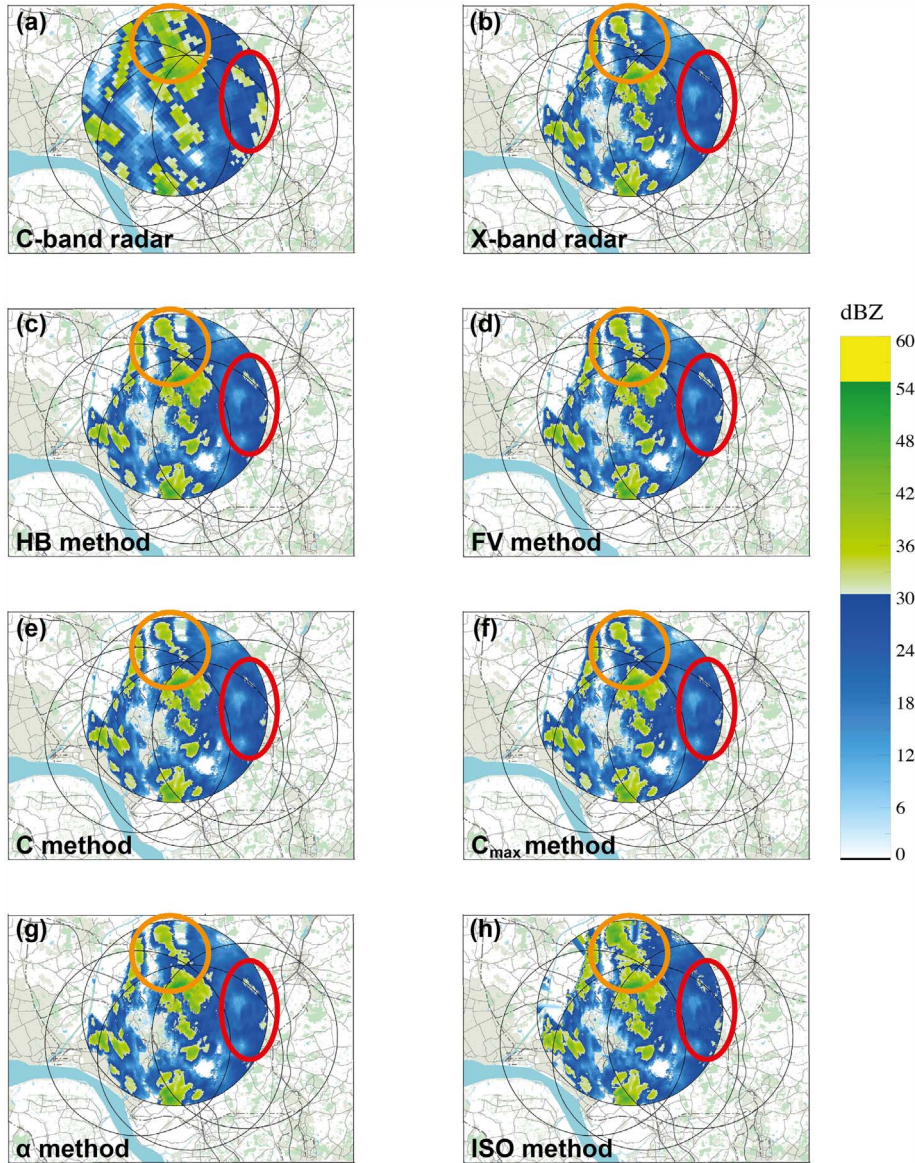


Fig. 2. Reflectivity scan for 15 May 2013 1830 UTC: (a) C-band radar observations, (b) uncorrected X-band radar observations, (c) HB method, (d) FV method, (e) C method, (f)  $C_{\max}$  method, (g)  $\alpha$  method and (h) ISO method.

C- and X-band radar systems usually measure reflectivity with different scanning strategies, spatial and temporal resolution. Therefore, when C-band observations are used for X-band attenuation correction they need to be spatially and temporally refined to the grid of the X-band radar and inter- or extrapolated in time (depending on whether it is for postprocessing or real-time applications) to match the X-band radar observations. In addition to different spatial and temporal resolution, both radar systems measure in different heights. However, in the overlapping area the height of the radar beam is lower than 1 km for both systems. The main source of error when comparing reflectivity measurements of different heights is the influence of the bright band. In this study, we use data from May to September, when the bright band is most likely located in heights greater than 1 km. Therefore, we neglect differences in altitude between C- and X-band radar measurements in this study.

Another issue with using two different radar systems for attenuation correction is that the methods become affected by differences in the calibration of the two radar systems. To avoid including C-band calibration errors to the correction, a modified version is tested for the C method that uses ratios of  $A$  at the first ( $r_0$ ) and the last ( $r_{\max}$ ) rainy range bin along the radar beam from Eq. (9):

$$A_{\text{mod}} = \frac{A(r_{\max})}{A(r_0)}. \quad (13)$$

Here,  $r_0$  is the first range bin of each radar beam in radial direction with reflectivities in X- and C-band larger than 10 dBZ and  $r_{\max}$  the last range bin with only C-band larger than 10 dBZ, because X-band measurements are attenuated by precipitation.

All algorithms described above are based on the statistical relation between true reflectivity  $Z$  and specific attenuation  $k$  with coefficients  $\alpha$  and  $\beta$  that depend on the radar wavelength. Furthermore, path integration of  $k$  and, therefore  $Z$ , presupposes continuous reflectivity measurements along each radar beam. Data gaps, caused by filtering of non-meteorological echoes have been interpolated.

As mentioned above Lengfeld et al. (2016) suggested another method based only on the ratio of reflectivity observations of X- and C-band radars. The path-integrated attenuation  $PIA$  at a range bin  $r$  is

$$PIA(r) = 10 \log[A(r)]. \quad (14)$$

For this method the logarithmic ratio of reflectivities from C-band radar,  $Z_{\text{Cband}}$ , and X-band radar,  $Z_m$ , is used to estimate the path-integrated attenuation (dB), called  $K$  hereafter:

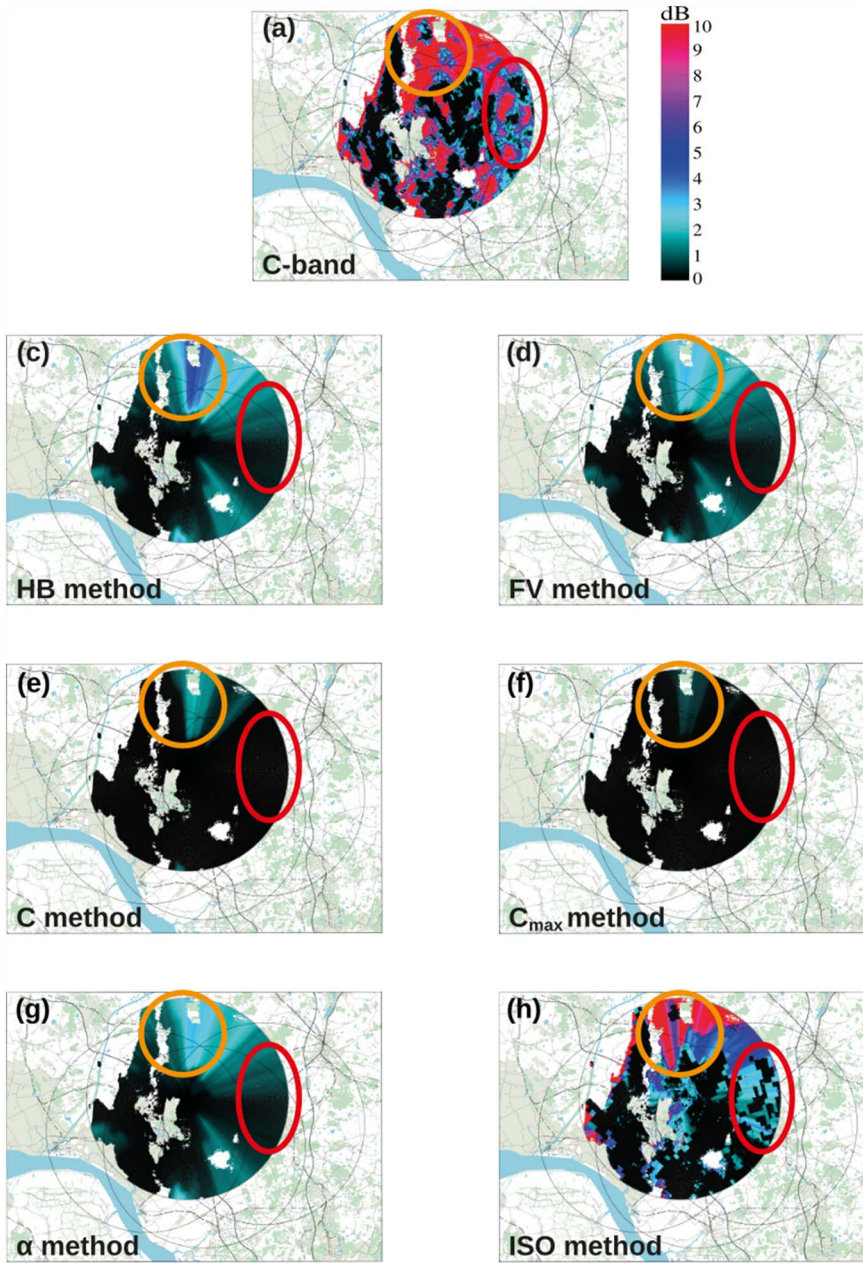


**Fig. 3.** Differences in reflectivity for 15 May 2013 1830 UTC between X-band radar observations and (a) C-band radar observations, (c) HB method, (d) FV method, (e) C method, (f)  $C_{\max}$  method, (g)  $\alpha$  method and (h) ISO method (numbering in accordance with Fig. 2).

$$K(r) = 10 \log \left[ \frac{Z_{Cband}(r)}{Z_m(r)} \right]. \quad (15)$$

In theory,  $K$  should increase (or stay constant in case of no rain) with range because reflectivity measurements of the C-band radar are less affected by attenuation than those of the X-band radar. In reality, however,  $K(r)$  is not always a monotonically increasing function due to temporal and spatial mismatch of the scan geometry, Mie effects and erroneous measurements in both radar systems, caused e.g. by external emitters or obstacles. To ensure continuous monotone, increasing functions of  $K$ , a simple unweighted linear isotonic regression (Barlow and Brunk, 1972), the so-called pool adjacent violators algorithm (PAVA) is applied to  $K$  along each radar beam, based on the following concept:

$$K_{IR}(n_i) = \max [K(n_i), K_{IR}(n_{i-1})] \quad \text{with} \quad i = 2, \dots, n, \quad (16)$$

with  $n$  being the number of range bins along the radar beam, and  $K_{IR}$  the isotonic regression for calculated values  $K(1), \dots, K(n)$ . The monotonically increasing function  $K_{IR}$  can then be added to the measured

reflectivity of the X-band radar in logarithmic units:

$$Z_{ISO}(r) = 10^{0.1[10 \log_{10}[Z_m(r)] + K_{IR}(r)]} = Z_m(r) 10^{0.1 K_{IR}(r)}. \quad (17)$$

The performance of the *ISO* method for attenuation correction will be compared to the original *HB* algorithm, methods *FV*,  $\alpha$  and *C* based on the  $k$ - $Z$ -relation, as well as the last algorithm using  $A_{mod}$  from Eq. (13) instead of  $A_{\max}$  (referred to as  $C_{\max}$  hereafter).

### 3. Radar systems and data set

The X-band radar used in this study is part of a network of five local area weather radars (LAWRs) set up north of Hamburg, Germany, and in the city centre (Fig. 1), within the project Precipitation and Attenuation Estimates from a High-Resolution Weather Radar Network (PATTERN). The LAWRs have a maximum range of 20 km and perform horizontal scans with a temporal resolution of 30 s, range resolution of 60 m and  $1^\circ$  angular sampling resolution. Their technical specifications are given in Table 2. Calibration was performed for a 3 month period using vertically pointing micro rain radars (MRRs) (Peters et al., 2005)

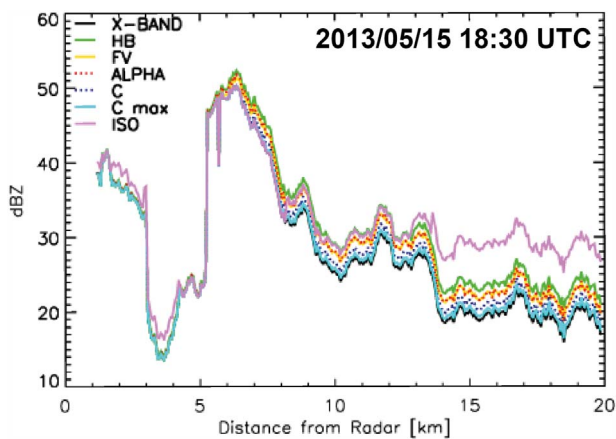


Fig. 4. Reflectivity along the radar beam at 15° azimuth for 15 May 2013 1830 UTC. Different colors and line styles denote different attenuation correction methods: black line for uncorrected X-band radar observations, green line for HB method, yellow line for FV method, dotted red line for  $\alpha$  method, dotted dark blue line for C method, light blue line for  $C_{\max}$  method and pink for ISO method. (For interpretation of the references to color in this figure legend, the reader is referred to the web version of this article.)

and rain gauges that are installed within the radar-covered area. MRR measurements from a different time period are also used here for evaluating the performance of each attenuation correction method. In contrast to comparisons with precipitation observations from ground-based rain gauges, using MRRs allows comparing directly measured reflectivities in a common volume and height. For more information on the X-band radars as well as the data processing, see Lengfeld et al. (2014).

The C-band radar is part of the radar network operated by the German Weather Service (DWD). It covers a radius of 128 km around the city of Hamburg and provides a reflectivity scan every 5 min with spatial resolution of 1 km and angular resolution of 1°. More technical details can be found in Table 2. The calibration of the C-band radar receiver is obtained from calibrated signal generators. The transmitter is calibrated with a power meter. The classical HB algorithm (Hitschfeld and Bordan, 1954) is applied for attenuation correction and comparison with MRR measurements showed good agreement between both systems (see Lengfeld et al., 2016).

For this study, reflectivity observations from the northernmost X-band radar of the network are used. The radar is located on a steel tower on the small military airport Hungrigr Wolf and, therefore, is called Hungrigr Wolf Tower (HWT).

Advantages and disadvantages of each attenuation correction method are examined for two case studies: a convective and a stratiform event. The convective event occurred on 15 May 2013 and last 9 h from 1300 to 2200 UTC. Small precipitation areas covered the catchment with reflectivities of up to 50 dBZ. The stratiform event of 19 June 2013 lasted 7 h from 1700 to 2400 UTC. During this event, a frontal system with a large area of heavy rainfall crossed the catchment. Additionally, a five month period from 1 May to 30 September 2013 is investigated for a longterm comparison of corrected X-band radar reflectivity and MRR observations.

#### 4. Comparison

First two case studies are investigated for a detailed study of the performance of each attenuation correction method: a convective and a stratiform event. Advantages and disadvantages of each method are addressed for a single radar scan of both events. Finally a longterm study of the attenuation factors for each method and a comparison with MRR data over 5 months of observations is carried out.

##### 4.1. Convective event: 15 May 2013 from 13 to 22 UTC

A radar scan from 1830 UTC is chosen as an example for this convective event (Fig. 2). The eastern half of the radar area is almost completely covered with precipitation. Reflectivities of up to 50 dBZ are observed by the C-band radar in Fig. 2a. The largest and strongest precipitation cell is located north of the radar marked by orange circles in Fig. 2. The X-band radar reflectivities (Fig. 2b) far away from the radar show much lower values because of path attenuation due to liquid water. The difference of C- and X-band radar data in Fig. 3a indicates underestimation of more than 10 dB in this area by the X-band radar. The same can be seen for areas of high reflectivities at the outer eastern part of the radar, encircled in red. On the other hand, the reflectivity field observed by the X-band radar shows much more detail and structure than the one observed by the C-band radar, because of its higher radial resolution.

The results of the attenuation correction algorithms introduced in Section 2 are presented in Fig. 2c–h and differences between corrected and measured X-band reflectivity are shown in Fig. 3c–h. Reflectivities along the radar beam of 15° azimuth in Fig. 4 emphasize the differences between the applied algorithms.

First the classic HB algorithm (Eq. (2)) is applied to the X-band radar observations. Qualitatively, the corrected reflectivity in Fig. 2c shows some improvement, especially in the northern part, but the HB algorithm underestimates the C-band reflectivity and is not able to reproduce, e.g., the areas of strong reflectivity within the red circle. In Fig. 4, comparison of measured (black line) and HB-corrected (green line) reflectivities along the 15° azimuth indicates that in the proximity of the radar no attenuation correction is done. At about 6 km distance from the radar, reflectivity observations reach a maximum of 50 dBZ, and from here onward the HB algorithm results in the highest reflectivities up to 12 km distance from the radar. Overall, the HB algorithm provides the largest corrections of all methods based on the k-Z-relation, resulting in a maximum PIA of 4 dB at 20 km distance. The difference between corrected and measured reflectivity scan in Fig. 3c indicates attenuation estimates up to 6 dB in the orange encircled area, but hardly any correction within the red circle. Here, the areas of high reflectivity are too small to produce large enough attenuation factors for adequate correction, but on the other hand do not cause any instabilities in this case either.

The FV, C,  $C_{\max}$  and  $\alpha$  methods (Fig. 2d–g) are more conservative in this case than the HB algorithm because they restrict the maximum possible attenuation, so that their attenuation factor is either equal to or smaller than for HB. Therefore, the reflectivity values are lower than for the HB algorithm. Differences between corrected and measured reflectivity for the FV and  $\alpha$  method in Fig. 3d and g are very similar and do not exceed 3.5 dB. The corrected reflectivity values obtained with the C method are even smaller than those of HB with differences of only up to 2.5 dB. This means that  $\epsilon$  from Eq. (12) is lower than 1. In case of no errors in radar calibration or in the estimate of PIA,  $\epsilon = 1$ . Using the ratio of X- and C-band reflectivities at the first and last rainy range bin in the  $C_{\max}$  method increases the underestimation even more, in this case with differences less than 1 dB. Fig. 4 underlines the similarity of FV (yellow line) and  $\alpha$  (red dotted line). Reflectivities of the C method (dotted dark blue line) are less than FV and  $\alpha$  and corrections using  $C_{\max}$  (light blue line) are smallest along the radar beam. All the methods based on the k-Z-relation underestimate the attenuation in this case.

Using the ratio of X- and C-band radars along the whole radar beam in the ISO algorithm leads to higher attenuation correction factors and, therefore, higher reflectivity values, especially in the northern area encircled in orange in Fig. 2h. Differences in Fig. 3h reach a maximum of 10 dB in this region. The higher resolved structure compared to the C-band radar is maintained because of the simple additive correction coefficients, but as the other methods, the ISO algorithm cannot reproduce the high reflectivity values in the red circle due to the regression performed. In Fig. 4 ISO (pink line) is the only algorithm that

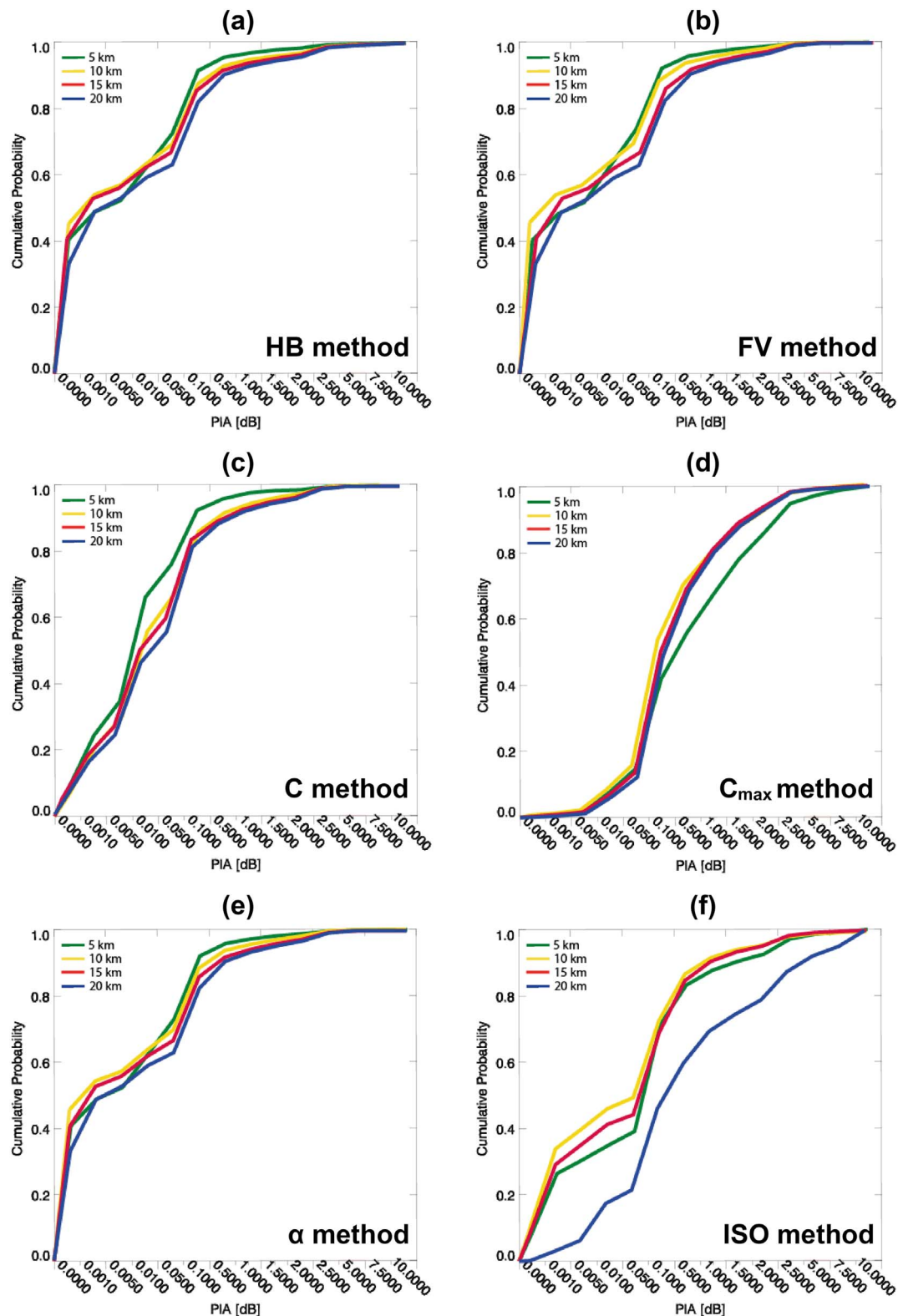


**Fig. 5.** Cumulative probability of path integrated attenuation (PIA) for 15 May 2013 1300–2200 UTC for (a) HB, (b) FV, (c) C, (d)  $C_{\max}$ , (e)  $\alpha$  and (f) ISO method. Different colors and line styles denote different distances from the radar: green line for 5 km, dashed yellow line for 10 km method, red line for 15 km and blue line for 20 km. (For interpretation of the references to color in this figure legend, the reader is referred to the web version of this article.)

raises the reflectivity values in the first 6 km. This is mainly caused by calibration differences between the two systems and to a smaller extend by Mie-effects or the temporal and spatial mismatch of both datasets, because the C-band radar data has been interpolated to match the X-band radar grid. From 12 km onward, ISO results in much higher

reflectivities than all other methods because it depends only on observed C-band radar measurements. These higher values cannot be reproduced by the methods based on the k-Z-relation.

However, Fig. 4 shows only the comparison of the different attenuation correction algorithms for a single azimuth angle at one time

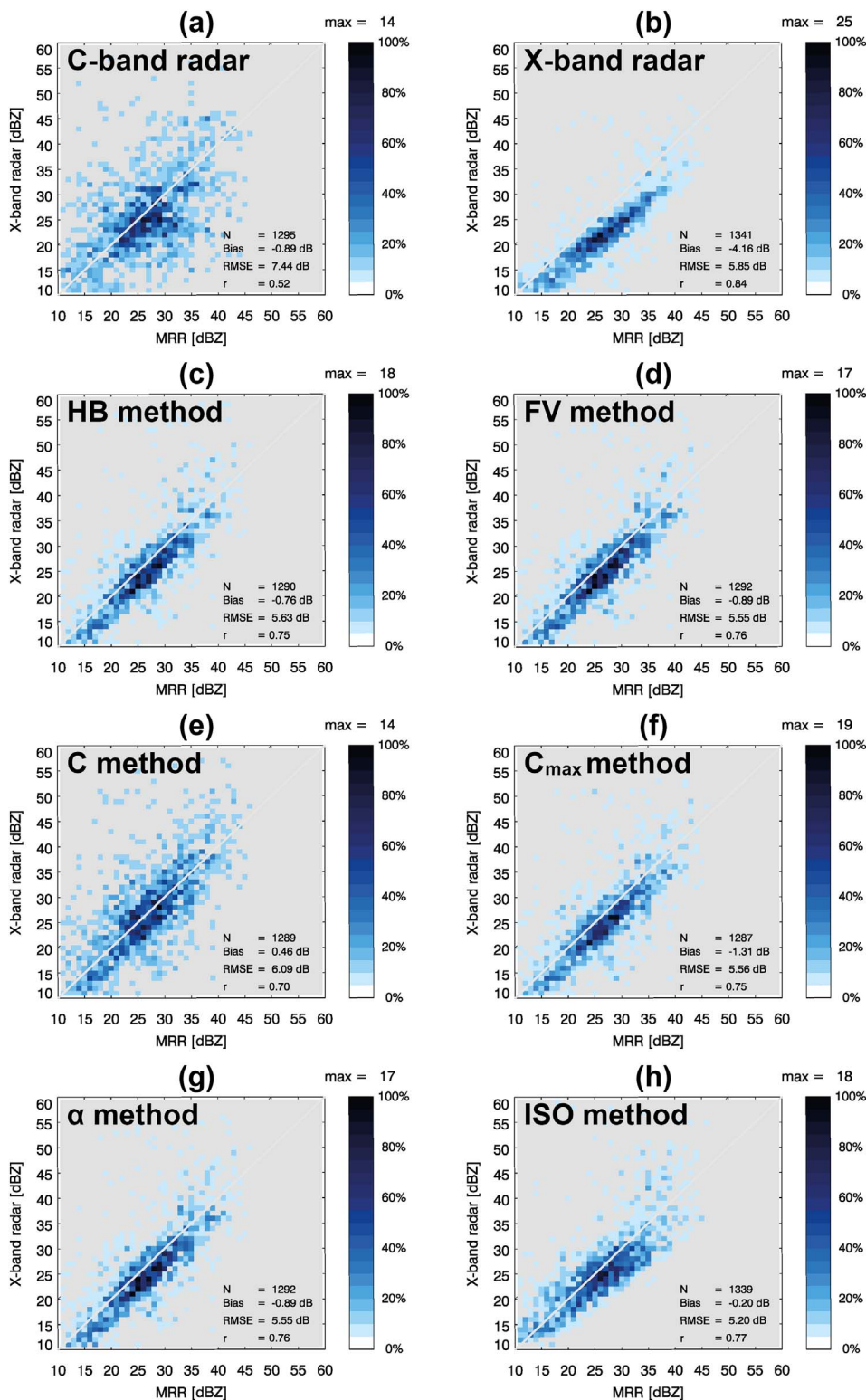


**Fig. 6.** Comparison of reflectivity observations from radar and MRRs for the convective case on 15 May 2013 1300–2200 UTC: (a) C-band radar observation, (b) uncorrected X-band radar observations, (c) HB method, (d) FV method, (e) C method, (f)  $C_{\max}$  method, (g)  $\alpha$  method, (h) ISO method.

step. For more general conclusions the cumulative probability of the  $PIA$  is investigated over all azimuth angles and the whole 9 h of the convective case of 15 May 2013. In Fig. 5 the cumulative probability of  $PIA$  at four different distances from the radar (5, 10, 15 and 20 km) is shown for all six algorithms. Maximum  $PIA$  for this event is 10 dB. This is in accordance with Delrieu et al. (2000) who found maximum ranges between 16 and 20 km for  $PIA$  values up to 10 dB. Results for HB, FV and  $\alpha$  in Fig. 5a, b and e are very similar. In around 40%,  $PIA$  is around 0 dB, meaning there is no or hardly any correction for attenuation. This

indicates light rain between the convective cells. Attenuation correction is rather small with  $0.001 \text{ dB} < PIA < 0.1 \text{ dB}$  in 15% and moderate with  $0.1 \text{ dB} < PIA < 0.5 \text{ dB}$  in 30% of the cases, corresponding to the convective cells. Only 5% of all  $PIA$  values are larger than 1 dB.

In case of homogeneous distribution of rainfall over the radar covered area, one would expect higher percentage of low  $PIA$  values closer to the radar than at larger distances. That means that the curves should be sorted from left to right in the following order: 5 km (green), 10 km (yellow), 15 km (red), 20 km (blue). As expected  $PIA$  is smallest at the

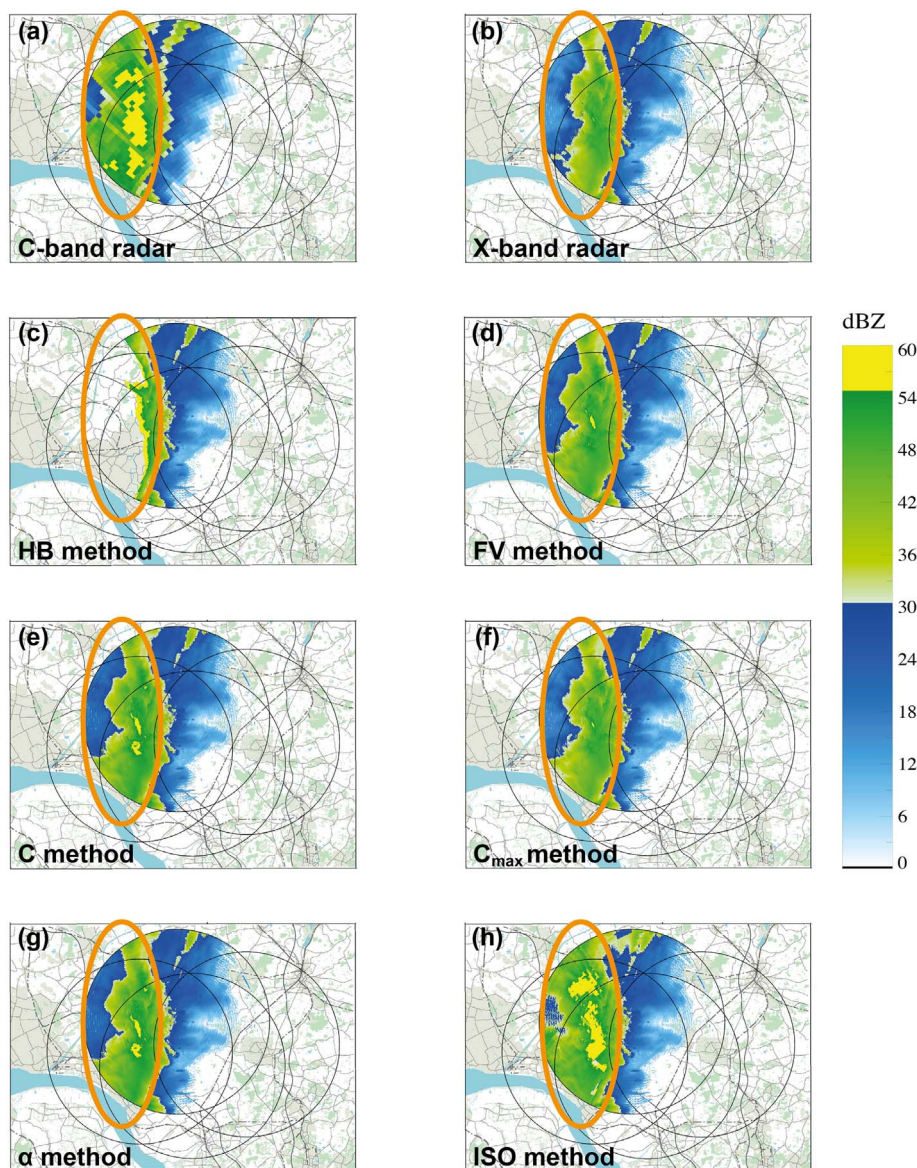
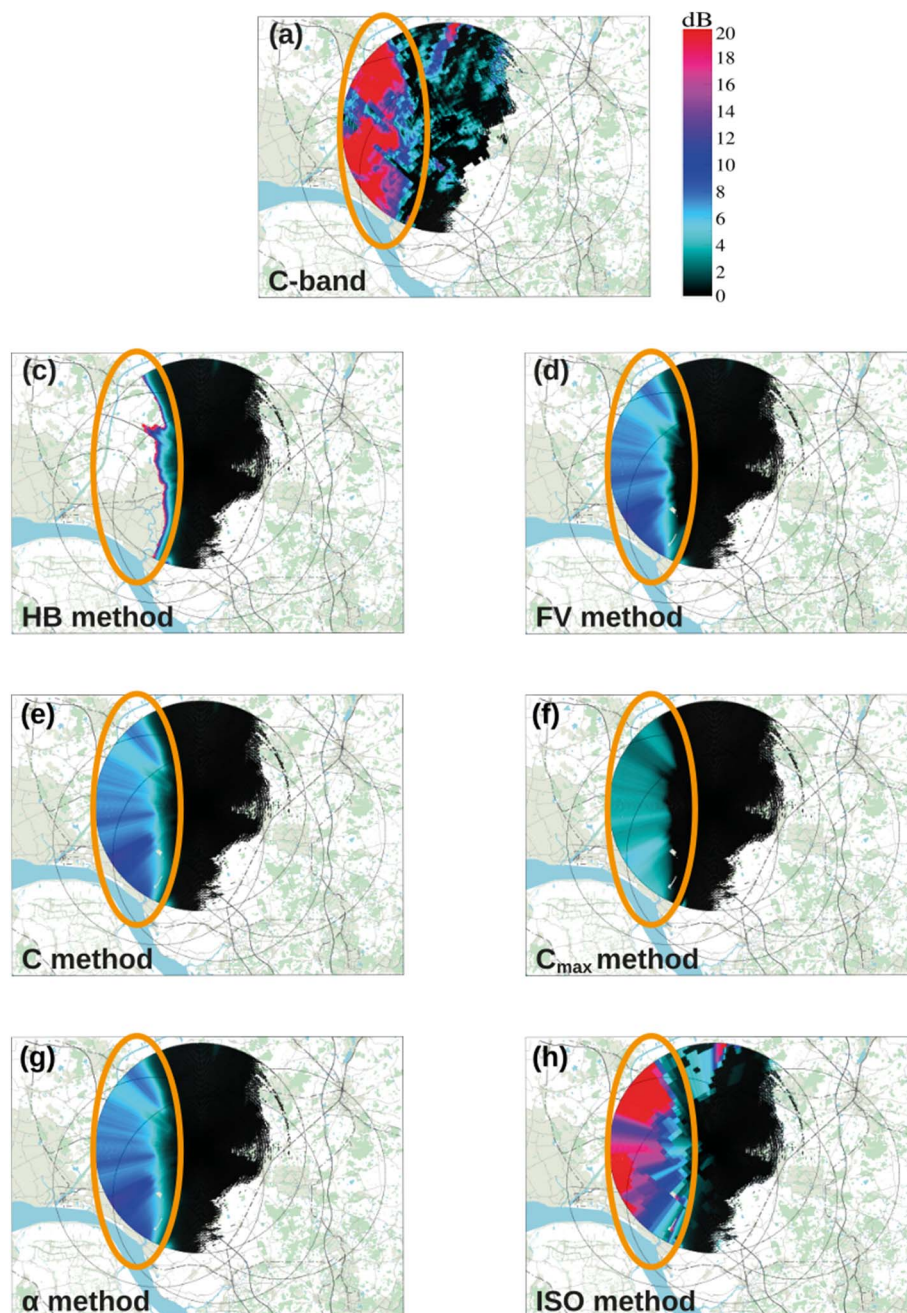


Fig. 7. Reflectivity scan for 19 June 2013 1915 UTC: (a) C-band radar observations, (b) uncorrected X-band radar observations, (c) HB method, (d) FV method, (e) C method, (f)  $C_{\max}$  method, (g)  $\alpha$  method and (h) ISO method.

shortest distance to the radar (5 km shown as green line) and increases with increasing distance, i.e. in general the percentage of higher  $PIA$ s increases with distance. Surprisingly there are less  $PIA$  values lower than 0.05 dB at 5 km than at 10 and 15 km. This could be due to the convective structure of the rain event. In these graphs, only areas with precipitation are included, which means that this statistic is dependent on the distribution of precipitation within the radar domain. A possible scenario would be a convective case with local development of more and stronger precipitation cells close to the radar and less and weaker or even no cells at larger distances. Because there are more cells near the radar, the percentage of high  $PIA$  values might be higher than at larger distances with less precipitation cells, simply because rain free areas are not considered in the calculation of the statistic. A simple example for such a scenario would be a case with two areas of precipitation: A strong precipitation cell at around 5 km north and a weaker precipitation cell at around 10 km south of the radar location. The remaining area is rain free and not considered in the statistic. In this scenario, there is an area of relatively high  $PIA$  values at 5 km distance compared to an area of lower  $PIA$  values at 10 km distance. Therefore, the percentage of low  $PIA$  values will be higher for 10 km than for 5 km and the yellow curve (10 km) would be shifted to the left towards lower  $PIA$  values compared to the green curve (5 km).

The C method performs attenuation correction in more than 80% of the cases, but with lower  $PIA$  values than the before mentioned methods ( $0 \text{ dB} \leq PIA < 0.05 \text{ dB}$  in 60% of the cases). The cumulative probability of  $PIA$  for  $C_{\max}$  indicates a bias between X- and C-band radar of 0.05 dB and 0.5 dB, because, in contrast to the methods before, more than 60% of the  $PIA$  values fall within this range and unlike for the other methods, the  $C_{\max}$  method performs attenuation correction for all range bins and time steps ( $PIA > 0.005$ ). This bias is most obvious at 5 km. Although the influence of attenuation increases with increasing distance to the radar, the percentage of larger  $PIA$  is higher at 5 km than at further distances. The influence of different calibrations of both radars seems to vanish with distance due to other disturbances along the radar beam (e.g., clutter or temporal and spatial mismatch between both systems). This is underlined by the ISO method which also shows a strong increase in probability for values between 0.1 dB and 0.5 dB. In contrast to  $C_{\max}$ , ISO does not perform any attenuation correction in 25% of the cases for distances of less than 20 km, when the X-band radar observations are equal to or higher than the C-band radar observations for reasons already discussed above. In contrast to all other methods,  $PIA$  values for 20 km distance are clearly larger than for 5, 10 and 15 km. This could be due to the fact, that in cases of negative dBZ values, measurements from the C-band radar are used while the other



**Fig. 8.** Differences in reflectivity for 19 June 2013 1915 UTC between X-band radar observations and (a) C-band radar observations, (c) HB method, (d) FV method, (e) C method, (f)  $C_{\max}$  method, (g)  $\alpha$  method and (h) ISO method (numbering in accordance with Fig. 7).

methods cannot perform any correction.

A comparison with reflectivity observations from seven MRRs that are located within the X-band radar network (Fig. 1) is presented in Fig. 6. The MRRs are vertically pointing radars that allow for a comparison with the horizontally scanning X- and C-band radars in a common volume. However, there is a temporal and spatial mismatch between the systems, because the MRRs measure with higher frequency (10 s) than the radars (30 s for X-band, 5 min for C-band) and the horizontal extension of the radar bins is larger than the MRR bins, especially for the C-band radar. Therefore, correlation (root mean square error (RMSE)) between C-band radar and MRRs in Fig. 6a is much lower (higher) than for the X-band radar in Fig. 6b. Nevertheless, the bias is rather small for C-band radar ( $-0.89$  dB) in comparison to the X-band radar which has a negative bias of  $-4.16$  dB probably mainly caused by attenuation. Applying attenuation correction reduces this bias significantly for all six methods to values between  $-1.31$  dB for  $C_{\max}$  in Fig. 6f and  $-0.2$  dB for ISO in Fig. 6h. Only the C algorithm

seems to slightly overestimate attenuation resulting in a positive bias of  $0.46$  dB. This is surprising because the difference between measured and corrected reflectivity for the exemplary scan in Fig. 3 was small. However, the C algorithm seems to be affected by calibration errors of the C-band radar leading to the overall overestimation in comparison to MRR observations and requires the application of  $C_{\max}$  that takes differences in calibration between X- and C-band radar into account. Overall, there seems to be more scattering in the data after applying the attenuation corrections. For the HB algorithm this is probably caused by the known problem of instability in case of large reflectivities. For the other methods it could be caused by the effect of using additional information from the C-band radar. Because of the coarser resolution in space and time, the accordance of MRRs and C-band radar is lower than for the X-band radar. Therefore, using the C-band radar data might introduce some uncertainty. Nevertheless, RMSE is slightly reduced for the methods based on the k-Z-relation (except for C) and noticeably reduced by 12% for ISO. The correlation decreases for all methods to

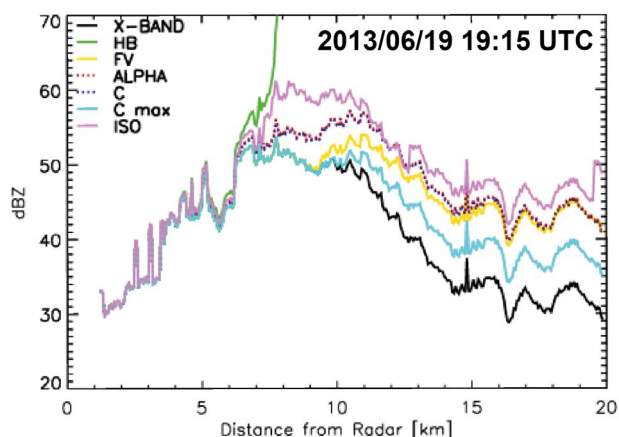


Fig. 9. Reflectivity along the radar beam at 240° azimuth for 19 June 2013 1915 UTC. Different colors and line styles denote different attenuation correction methods: black line for uncorrected X-band radar observations, green line for HB method, yellow line for FV method, dotted red line for  $\alpha$  method, dotted dark blue line for C method, light blue line for  $C_{\max}$  method and pink for ISO method. (For interpretation of the references to color in this figure legend, the reader is referred to the web version of this article.)

0.7 for C and 0.77 for ISO, but still remains clearly higher than for the C-band radar.

Overall, all six attenuation correction methods provide stable results in this convective case. Except for the C method that overestimates attenuation and enhances the RMSE, all algorithms result in an improvement in comparison with MRR observations. The original HB algorithm outperforms all other methods in the scan used for illustration shown in Fig. 2, but considering the whole event, HB, FV,  $C_{\max}$  and  $\alpha$  show similar results. Slightly better results are achieved with the ISO method.

#### 4.2. Stratiform event: 19 June 2013 from 17 to 24 UTC

In the illustrating scan for the stratiform event (1915 UTC), the western and central part of the radar is covered with rain (Fig. 7). The C-band radar observations (Fig. 7a) indicate reflectivities of up to 60 dBZ. These high values encircled in orange cannot be reproduced by the X-band radar (Fig. 7b). Here only reflectivities of up to 50 dBZ are observed. The differences between C- and X-band radar in Fig. 8a reach values of 20 dB in this area. A clear influence of attenuation can also be seen in the very northern part of the radar covered area.

In this stratiform event, the HB algorithm in Fig. 7c gets unstable due to high attenuation. This is a well-known problem of this method. Therefore, restricted algorithms are obligatory for attenuation correction in cases like this. FV, C and  $\alpha$  methods give very similar results, whereby the latter two are closer to the high reflectivity values indicated by the C-band radar. The reflectivity profile along the radar beam at 240° azimuth in Fig. 9 highlights this behaviour. Attenuation correction starts at around 7 km from the radar for HB (green line) and gets unstable within a kilometer distance. For  $\alpha$  (dotted red line) and FV (dotted blue line) the correction also starts at around 7 km, but for FV (yellow line) it does not start before kilometer 9. From 14 km onward, all three methods derive very similar results. The differences between corrected and measured X-band reflectivity in Fig. 8d, e and g display values of PIA of up to 12 dB. Using the restriction with C-band radar measurements for  $C_{\max}$  in Fig. 7f leads to less attenuation correction and, hence lower reflectivities and differences between X- and C-band radar observations in Figs. 7f and 8f, respectively. Although all methods account for attenuation, none of the algorithms based on the k-Z-relation is capable of reproducing the high reflectivity values observed by the C-band radar. This can only be achieved by the ISO method that directly uses the relation of X- and C-band radar measurements (Fig. 7h). The differences between corrected and measured X-band

reflectivity in Fig. 8h reach a maximum of more than 20 dB. The profile for ISO (pink line in Fig. 9) indicates that this method results in more than 50% stronger attenuation than the other algorithms, especially in the area of highest reflectivities between 8 and 11 km distance to radar.

The cumulative probability of the PIA for the whole stratiform event is shown in Fig. 10. Again, HB, FV and  $\alpha$  lead to very similar results, in Fig. 10a, b and e, respectively. These three methods do not or hardly correct for attenuation in more than 25% of the time ( $PIA \leq 0.001$  dB). In contrast to the convective event in the previous section in almost 15% of the cases attenuation correction is larger than 2 dB corresponding to the band of high reflectivities ( $> 50$  dBZ) encircled in Fig. 2, whereas HB has the highest amount of  $PIA \geq 2$  dB. Note that for HB this also includes cases in which the HB algorithm gets unstable. The C algorithm performs attenuation correction in 80% of the time.  $C_{\max}$  is consistent with the convective case and indicates again a bias of around 10% between X- and C-band radar with the strongest increase at  $PIA = 0.1$  dB. ISO performs attenuation correction in 90% of the time with more values between 0.005 and 0.5 dB (35%) but less values larger than 1 dB compared to the other methods. For all methods, PIA values are smallest at a distance of 5 km from the radar and increase with distance to the radar.

The comparison with MRR measurements in Fig. 11 shows again the influence of attenuation in the X-band radar observations. The bias between C-band radar and MRRs is only  $-0.21$  dB (Fig. 11a), while the X-band radar underestimates the MRR measurements by more than 5 dB (Fig. 11b). Nevertheless, the X-band radar observations correlate slightly better with the MRRs due to higher spatial and temporal resolution (correlation coefficient of 0.59 for C-band, 0.64 for X-band). The FV and the  $\alpha$  algorithm (Fig. 11d and g) almost eliminate the bias ( $-0.1$  dB), enhance the correlation coefficient to 0.72 and reduce the RMSE by a third to 4.95 dB and 4.93 dB, respectively. HB tends to overestimate attenuation with a positive bias of 0.31 dB. Due to instabilities of the algorithm this comparison contains around 50 data points less than the others. The C algorithm overcorrects by almost 3.6 dB and needs to be restricted with additional C-band radar data by using  $C_{\max}$  instead. But even using this additional information from C-band radar data does not outperform the FV and  $\alpha$  method. Applying the ISO algorithm leads to highest correlation of 0.76 between X-band and MRR data, but still underestimates the MRR measurements by almost 0.6 dB.

#### 4.3. Longterm study

In the previous sections, two different precipitation events have been investigated. In order to evaluate the longterm performance of each attenuation correction algorithm, all rain events between 01 May and 30 September 2013 are examined in this section and results are again compared to MRR measurements.

First, the cumulative probability of the attenuation factor for the whole period is displayed in Fig. 12. As already seen for the two case studies (Figs. 5 and 10), the PIA does not exceed 10 dB for a maximum range of 20 km as already shown by Delrieu et al. (2000) for case studies of three rain events in a Mediterranean region in France. They found that the PIA does not exceed 10 dB for maximum ranges between 16 and 20 km in 99% of the rain events considered in their study. In general, the curves are less dominated by single events or precipitation cells resulting in a smoother shape than for the convective and stratiform case studies. The HB, FV and  $\alpha$  methods in Fig. 12a, b and e provide similar results. (Note, that instabilities in the HB algorithm are not included in the cumulative probability). These three methods are also the most conservative, not correcting for attenuation in around 30% of the time when the rain rate is rather low. PIA with values of more than 0.1 dB only occur in less than 10% of the time. The C algorithm in Fig. 12c is less conservative. This algorithm results in PIA values larger than 0 dB in more than 95% of the cases. The bias between both radar systems is taken into account by the  $C_{\max}$  algorithm,

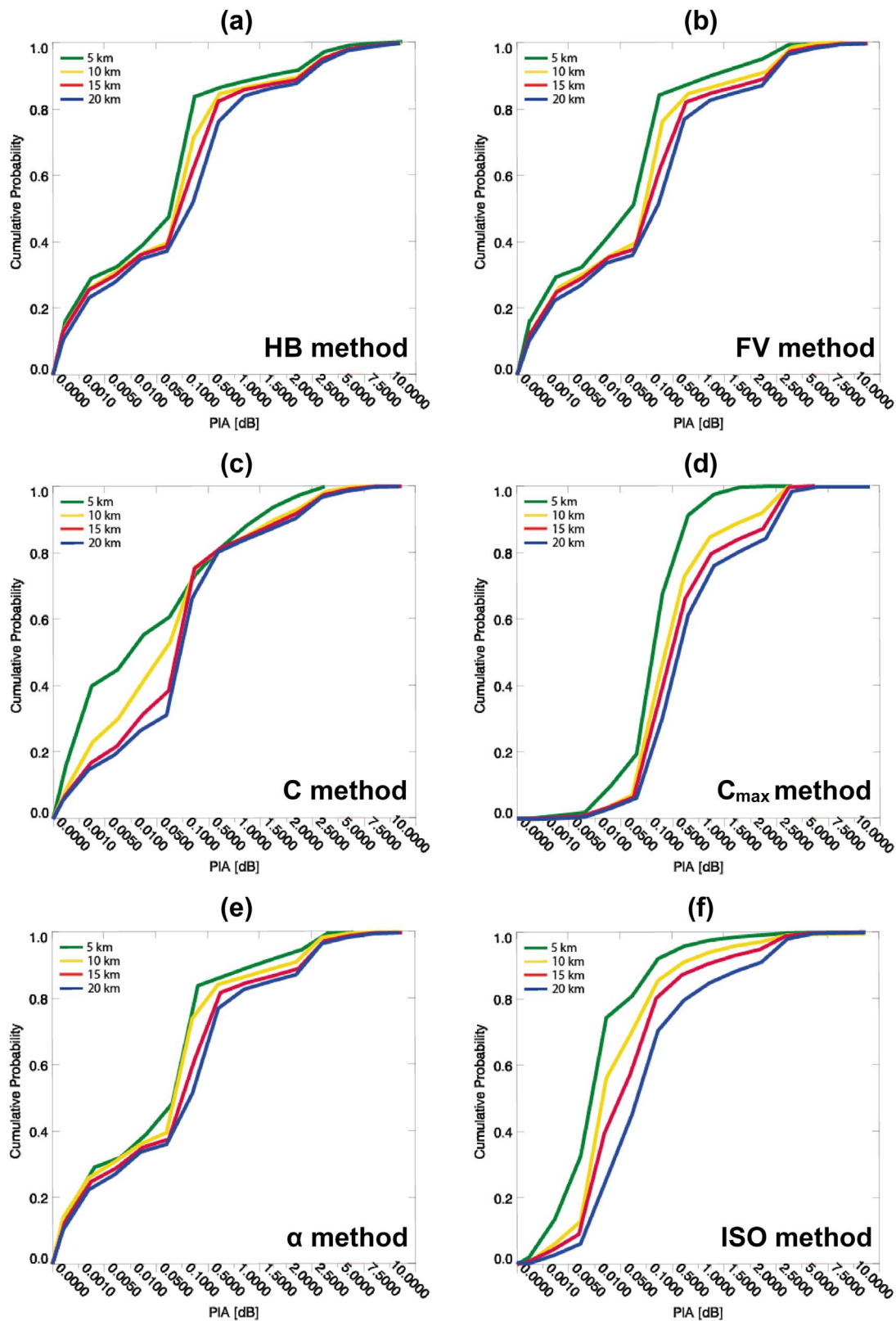


**Fig. 10.** Cumulative probability of path integrated attenuation (PIA) for 19 June 2013 1700–2400 UTC for (a) HB, (b) FV, (c) C, (d)  $C_{\max}$ , (e)  $\alpha$  and (f) ISO method. Different colors and line styles denote different distances from the radar: green line for 5 km, dashed yellow line for 10 km method, red line for 15 km and blue line for 20 km. (For interpretation of the references to color in this figure legend, the reader is referred to the web version of this article.)

resulting in a strong increase for PIA values between 0.1 and 0.5 dB. It seems that the correction for this method is dominated by the bias between both systems because PIA values are very similar for all four distances. ISO (Fig. 12f) also considers the bias between X- and C-band

but in contrast to  $C_{\max}$  that only takes into account observations at range bin  $r_{\max}$ , it uses C-band radar data for each individual radar bin along the beam.

The comparison with reflectivity observations from MRRs is shown

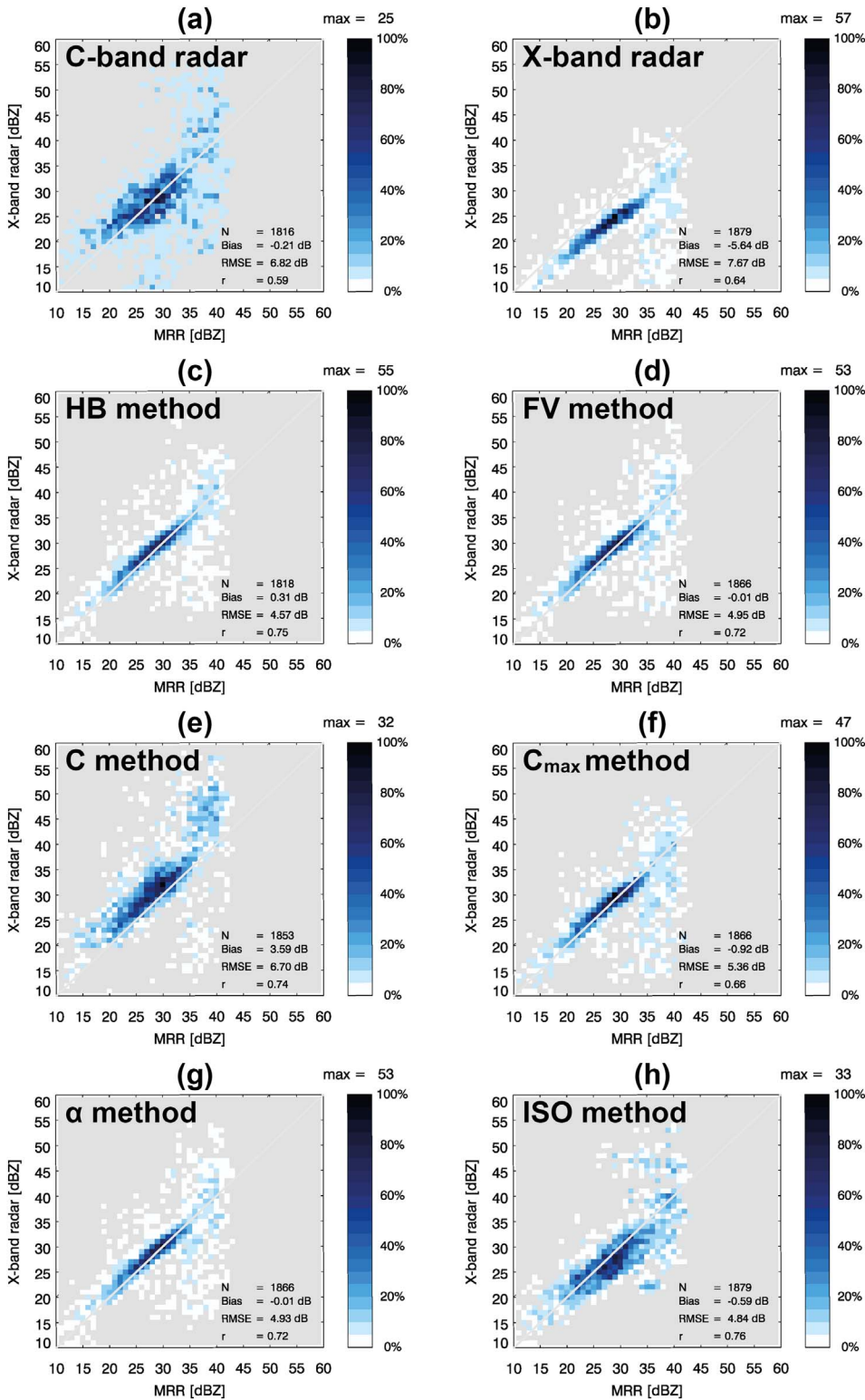


**Fig. 11.** Comparison of reflectivity observations from radar and MRRs for the stratiform case on 19 June 2013 1700–2400 UTC: (a) C-band radar observations, (b) uncorrected X-band radar observations, (c) HB method, (d) FV method, (e) C method, (f)  $C_{\max}$  method, (g)  $\alpha$  method, (h) ISO method.

in Fig. 13. In comparison to the C-band radar in Fig. 13a, the X-band radar in Fig. 13b is clearly influenced by attenuation resulting in an overall underestimation of  $-2.65$  dB, especially for reflectivity higher than  $25$  dB. Despite this underestimation X-band radar and MRRs are very well correlated with a correlation factor of  $0.9$ . All attenuation correction algorithms (except for C in Fig. 13e), reduce the RMSE from  $3.87$  dB for measured reflectivities in Fig. 13b by more than  $20\%$  to around  $3$  dB and maintain the high correlation. HB, FV and  $\alpha$  slightly overcorrect the reflectivity data resulting in positive biases between X-

band and MRRs between  $0.18$  dB and  $0.2$  dB. Note that instabilities of the HB algorithm are not included in this comparison. They would lead to a much stronger positive bias, larger RMSE and lower correlation factor. Only the C algorithm in Fig. 13e clearly overestimated the attenuation with an overall bias of  $2.25$  dB. This can be prevented by using the restriction of the  $C_{\max}$  method.  $C_{\max}$  provides the best results along with the ISO algorithm with a marginal bias of  $0.04$  dB and  $-0.03$  dB, respectively, for the whole five month period. This longterm study highlights (although not clearly obvious from the case study) the

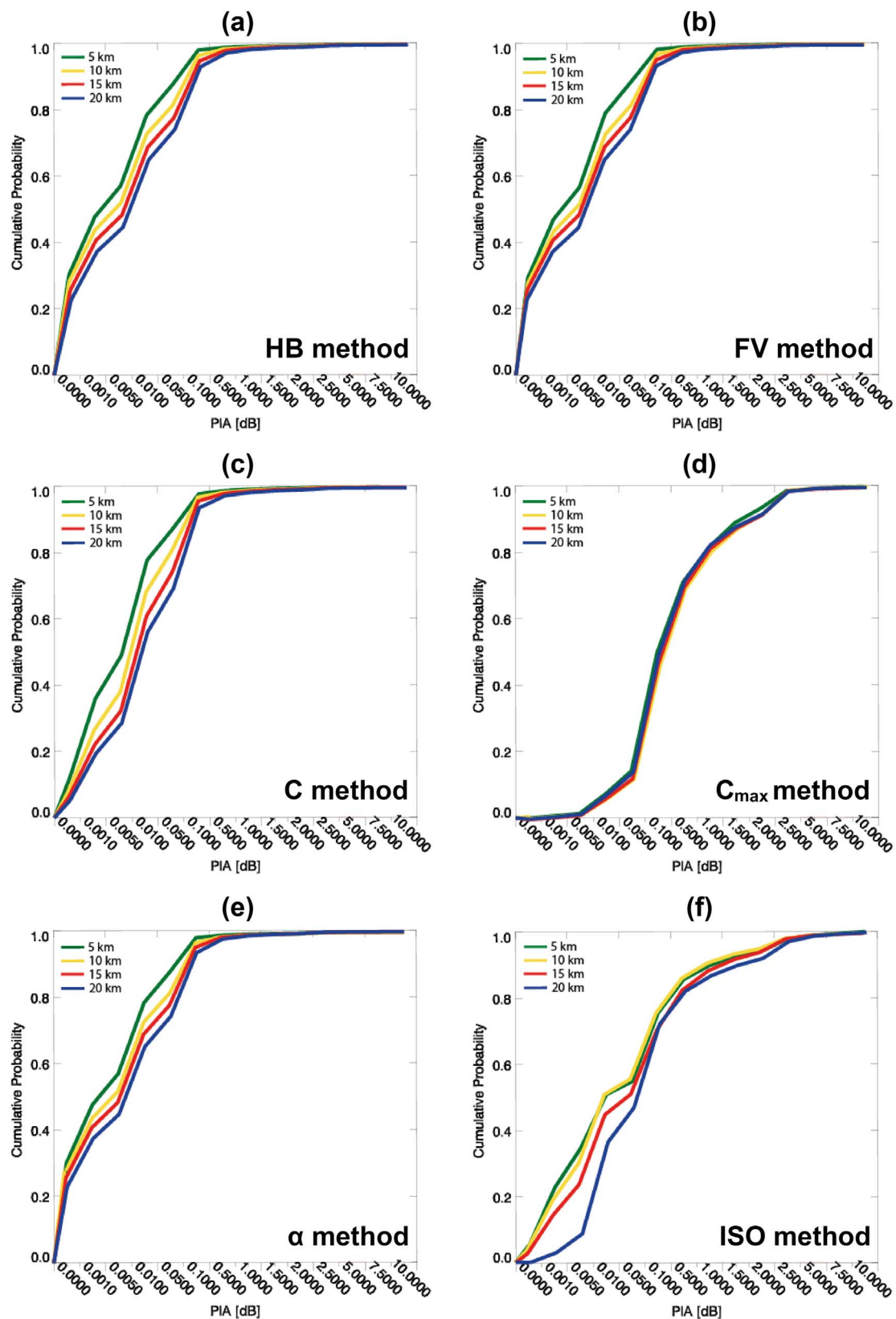


**Fig. 12.** Cumulative probability of path integrated attenuation (PIA) for 01 May to 30 September 2013 for (a) HB, (b) FV, (c) C, (d) C<sub>max</sub>, (e)  $\alpha$  and (f) ISO method. Different colors and line styles denote different distances from the radar: green line for 5 km, dashed yellow line for 10 km method, red line for 15 km and blue line for 20 km. (For interpretation of the references to color in this figure legend, the reader is referred to the web version of this article.)

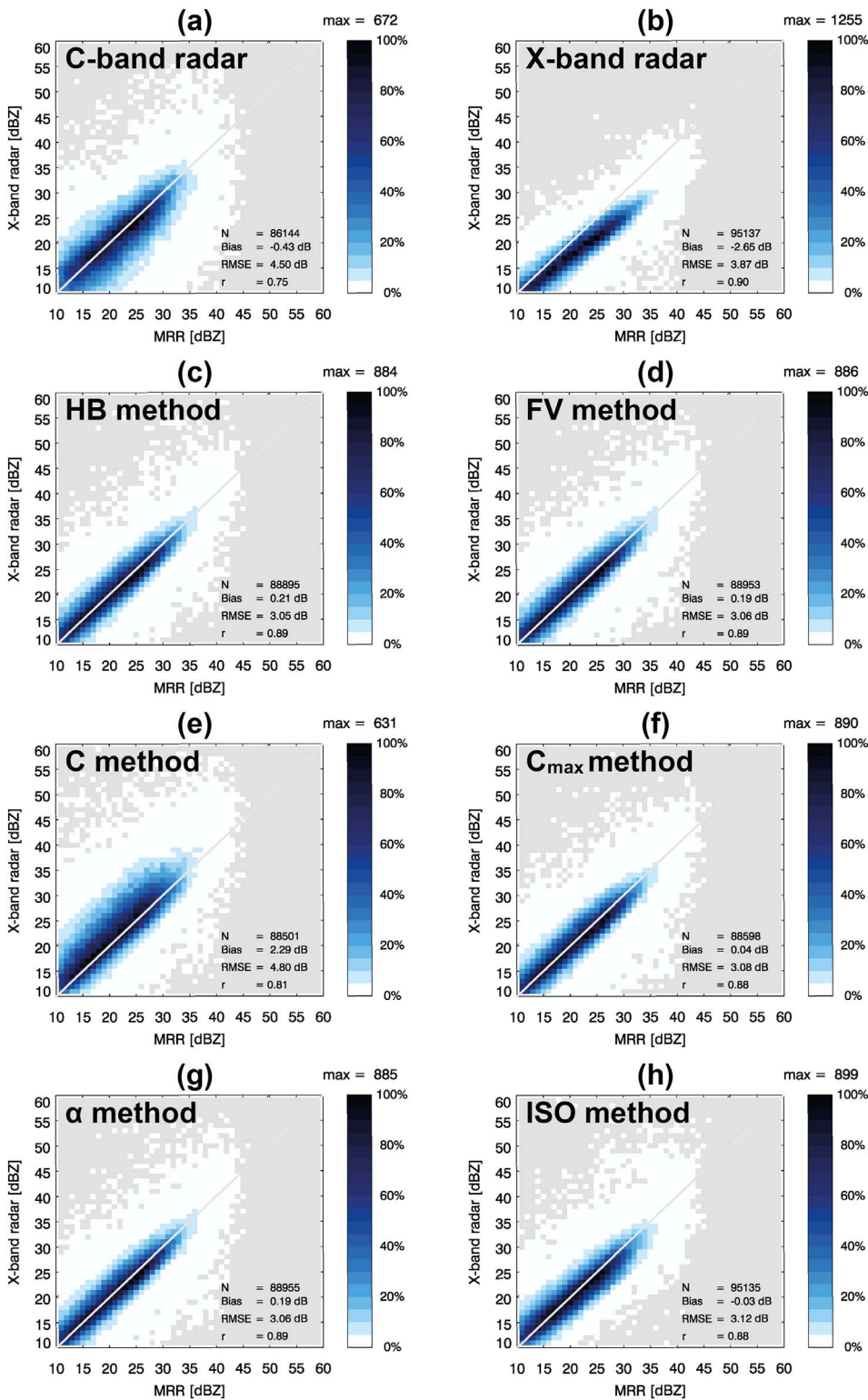


**Fig. 13.** Comparison of reflectivity observations from radar and MRRs for all rain events between May and September 2013: (a) C-band radar observations, (b) uncorrected X-band radar observations, (c) HB method, (d) FV method, (e) C method, (f)  $C_{max}$  method, (g)  $\alpha$  method, (h) ISO method.

importance of using additional information from C-band radar not only at the outermost range bin as a restriction in attenuation correction for X-band radar observations.

## 5. Conclusions

In this paper, the performance of six attenuation correction methods for individual X-band radars is examined and compared. Single-polarized X-band radars are a promising cost effective tool to complement

nationwide radar networks in areas of low coverage, e.g. due to blockage by mountains, or regions of special interest, e.g. urban areas. They are easy to install due to their small antenna size and provide precipitation observations in high temporal (up to 30 s) and spatial (< 100 m) resolution. The downside is high influence of attenuation by liquid water compared to C- or S-band radars. Dual-polarization radars could improve the data quality but they are much more expensive than single-polarization systems. Therefore, a good and stable algorithm for attenuation correction is crucial.

The original attenuation correction algorithm (*HB*) proposed by Hitschfeld and Bordan (1954) is the first method investigated in this study. It is based on the statistical relation between reflectivity and attenuation and is known to perform well in case of low precipitation and, therefore, low attenuation, but to get unstable in case of heavy precipitation and high attenuation. Therefore, three different methods proposed by Iguchi and Meneghini (1994) are also investigated: The final value (*FV*) method, that includes a restriction either obtained from ground echo in case of airborne radars or by mountain returns in case of horizontally pointing radars. In this study the mountain return is substituted by using measurements from less attenuated measurements from overlapping C-band radars at the maximum range bin of the X-band radar. The second solution adjusts the  $\alpha$  coefficient, the third solution the radar constant *C*. Additionally, the ratio between X- and C-band radar measurements at the X-band radar is included ( $C_{\max}$  algorithm) to avoid inducing uncertainties due to differences in the calibration of the two systems. The last algorithm investigated is the isotonic regression method proposed by Lengfeld et al. (2016). It is independent of the statistical k-Z-relation and directly makes use of the ratio between X- and C-band radar measurements.

First two case studies, a convective and a stratiform event, are investigated. In both cases observations from X-band radars are clearly affected by attenuation due to liquid water. They have a negative bias compared to micro rain radar (MRR) measurements of  $-4.16$  dB and  $-5.64$  dB in the convective and the stratiform case, respectively. Despite this attenuation-induced bias X-band radar observations are in better agreement with MRR measurements than the corresponding C-band radar observations in terms of correlation coefficients due to their higher spatial and temporal resolution. Application of all six attenuation correction methods to the X-band radar data leads to improvements.

In the convective case the bias compared to the MRRs is reduced by 80% for *HB*, *FV* and  $\alpha$ . The *C* method overcorrects for attenuation resulting in a positive bias of 0.46 dB. Therefore, eliminating the uncertainties in calibration by using  $C_{\max}$  is necessary. Best results are obtained by the isotonic regression method with a bias of only  $-0.2$  dB. Correlation is reduced by around 10% for all six methods to between 0.7 for *C* and 0.77 for *ISO* but is still distinctly higher than for C-band radar ( $r = 0.52$ ).

For the stratiform event the *HB* algorithm gets unstable. Best results are obtained by applying *FV* and  $\alpha$ . Both eliminate the negative bias caused by attenuation, reduce the *RMSE* by 35% and enhance the correlation to 0.72. The *ISO* method enhances the correlation even further to 0.76 but still results in a negative bias of  $-0.59$  dB. As for the convective event, the *C* method again overcorrects for attenuation and needs to be restricted by applying  $C_{\max}$ .

The same behaviour can be seen in a longterm study including all precipitation events from 01 May to 30 September 2013. The *C* method clearly overcorrects the attenuation effect resulting in a positive bias of 2.29 dB compared to MRR measurements. A slightly positive bias is obtained by *FV*,  $\alpha$  and *HB*. Applying the *ISO* and  $C_{\max}$  algorithms leads to the best results in terms of bias with  $-0.03$  dB and 0.04 dB, respectively. That shows that using information from a less attenuated radar not only at the outer ranges of the attenuated X-band radar, but also close to the radar, has a beneficial effect on the attenuation correction.

It has been shown that applying attenuation correction to high-resolution X-band radar observations restricted by C-band radar measurements lead to stable and qualitative reflectivity data that could be a beneficial addition to nationwide radar networks. For future studies the benefit of combining different methods should be examined. Due to the use of C-band radar data with temporal resolution of 5 min these algorithms are only applicable for post processing. In order to utilize them in real-time application, the algorithms need to be combined with a nowcasting scheme for the C-band radar data. Furthermore, the influence of differences in beam height between both systems should be

taken into account when applying the correction methods to wintertime data, where the bright band might influence reflectivity measurements.

## Acknowledgments

This work has been done in the framework of the project *Improving Hydrological Forecasting Using High-Resolution X-Band Radars* funded by the Deutsche Forschungsgemeinschaft (grant LE 3360/2-1). Co-authors are supported by the Spanish project FFHafZ (CGL2014-60700R).

The authors thank Prof. Felix Ament and Dr. Marco Clemens from the Meteorological Institute of the University of Hamburg for providing the X-band radar data and the German Meteorological Service (DWD) for providing the C-band radar data.

## References

- Atlas, D., Ulbrich, C.W., 1977. Path- and area-integrated rainfall measurement by microwave attenuation in the 1–3 cm band. *J. Appl. Meteor.* 16 (12), 1322–1331. [http://dx.doi.org/10.1175/1520-0450\(1977\)016<1322:PAIRM>2.0.CO;2](http://dx.doi.org/10.1175/1520-0450(1977)016<1322:PAIRM>2.0.CO;2).
- Barlow, R.E., Brunk, H.D., 1972. The isotonic regression problem and its dual. *J. Am. Stat. Assoc.* 67 (337), 140–147. <http://dx.doi.org/10.2307/2284712>.
- Beck, J., Bousquet, O., 2013. Using gap-filling radars in mountainous regions to complement a national radar network: improvements in multiple-Doppler wind synthesis. *J. Appl. Meteor. Climatol.* 52 (8), 1836–1850. <http://dx.doi.org/10.1175/JAMC-D-12-0187.1>.
- Berenguer, M., Park, S., Sempere-Torres, D., Didszun, J., Pool, M., Pfeifer, M., 2012. RAINSCANNER@Barcelona: an experiment to assess the hydrological value of a portable X-band radar. In: 7th European Conference on Radar Meteorology and Hydrology, Toulouse, France.
- Berne, A., Uijlenhoet, R., 2006. Quantitative analysis of X-band weather radar attenuation correction accuracy. *Nat. Hazards Earth Syst. Sci.* 6 (3), 419–425. <http://dx.doi.org/10.5194/nhess-6-419-2006>.
- Bringi, V.N., Balakrishnan, N., Zmric, D.S., 1990. An examination of propagation effects in rainfall on polarimetric variables at microwave frequencies. *J. Atmos. Ocean. Technol.* 7, 829–840.
- Chen, H., Chandrasekar, V., 2012. High resolution rainfall mapping in Dallas-Fort Worth urban demonstration network. IEEE International Geoscience and Remote Sensing Symposium: Proceedings 1936–1939. <http://dx.doi.org/10.1109/IGARSS.2012.6351123>.
- Delrieu, G., Andrieu, H., Creutin, J.D., 2000. Quantification of path-integrated attenuation for X- and C-band weather radar systems operating in mediterranean heavy rainfall. *J. Appl. Meteorol.* 39 (6), 840–850. [http://dx.doi.org/10.1175/1520-0450\(2000\)039<0840:QOPIAF>2.0.CO;2](http://dx.doi.org/10.1175/1520-0450(2000)039<0840:QOPIAF>2.0.CO;2).
- Delrieu, G., Caoual, S., Creutin, J.D., 1997. Feasibility of using mountain return for the correction of ground-based X-band weather radar. *J. Atmos. Oceanic Technol.* 14 (3), 368–385. [http://dx.doi.org/10.1175/1520-0426\(1997\)014<0368:FOUMRF>2.0.CO;2](http://dx.doi.org/10.1175/1520-0426(1997)014<0368:FOUMRF>2.0.CO;2).
- Feng, L., Xiao, H., Wen, G., Li, Z., Sun, Y., Tang, Q., Liu, Y., 2016. Rain attenuation correction of reflectivity for X-band dual-polarization radar. *MDPI Atmosphere* 7, 164. <http://dx.doi.org/10.3390/atmos7120164>.
- Figuras I Ventura, J., Tabary, P., 2013. The new French operational polarimetric radar rainfall rate product. *J. Appl. Meteor. Climatol.* 52 (8), 1817–1835. <http://dx.doi.org/10.1175/JAMC-D-12-0179.1>.
- Gunn, K.L.S., East, T., 1954. The microwave properties of precipitation particles. *Quart. J. Roy. Meteor. Soc.* 80, 522–545. <http://dx.doi.org/10.1002/qj.49708034603>.
- Hitschfeld, W., Bordan, J., 1954. Errors inherent in the radar measurement of rainfall at attenuating wavelengths. *J. Meteorol.* 11 (1), 58–67. [http://dx.doi.org/10.1175/1520-0469\(1954\)011<0058:EIITRM>2.0.CO;2](http://dx.doi.org/10.1175/1520-0469(1954)011<0058:EIITRM>2.0.CO;2).
- Iguchi, T., Meneghini, R., 1994. Intercomparison of single-frequency methods for retrieving a vertical rain profile from airborne or spaceborne radar data. *J. Atmos. Oceanic Technol.* 11 (6), 1507–1516. [http://dx.doi.org/10.1175/1520-0426\(1994\)011<1507:IOSFMF>2.0.CO;2](http://dx.doi.org/10.1175/1520-0426(1994)011<1507:IOSFMF>2.0.CO;2).
- Lengfeld, K., Clemens, M., Merker, C., Muenster, H., Ament, F., 2016. A simple method for attenuation correction in local X-band radar measurements using C-band radar data. *J. Atmos. Oceanic Technol.* 33 (11), 2315–2329. <http://dx.doi.org/10.1175/JTECH-D-15-0091.1>.
- Lengfeld, K., Clemens, M., Muenster, H., Ament, F., 2014. Performance of high-resolution X-band weather radar networks — the PATTERN example. *Atmosph. Measur. Tech.* 7 (12), 4151–4166. <http://dx.doi.org/10.5194/amt-7-4151-2014>.
- Matrosov, S., Cifelli, R., Gochis, D., 2013. Measurements of heavy convective rainfall in the presence of hail in flood-prone areas using an X-band polarimetric radar. *J. Appl. Meteor.* 52 (2), 395–407. <http://dx.doi.org/10.1175/JAMC-D-12-052.1>.
- Meneghini, R., Eckerman, J., Atlas, D., 1983. Determination of rain rate from a spaceborne radar using measurements of total attenuation. *IEEE Trans. Geosci. Remote Sens.* 21, 34–43. <http://dx.doi.org/10.1109/TGRS.1983.350528>.
- Ochoa-Rodriguez, S., Wang, L.-P., Gires, A., Pina, R.D., Reinoso-Rondinel, R., Bruni, G., Ichiba, A., Gaitan, S., Cristiano, E., van Assel, J., Kroll, S., Muria-Tuyls, D., Tisserand, B., Schertzer, D., Tchiguirinskaia, I., Onof, C., Willems, P., ten Veldhuis, M.-C., 2015. Impact of spatial and temporal resolution of rainfall inputs on urban hydrodynamic modelling outputs: a multi-catchment investigation. *J. Hydrol.* 531, 389–407. <http://dx.doi.org/10.1016/j.jhydrol.2015.05.035>.

- Peters, G., Fischer, B., Muenster, H., Clemens, M., Wagener, T., 2005. Profiles of raindrop size distributions as retrieved by micro rain radars. *J. Appl. Meteorol.* 44 (12), 1930–1949. <http://dx.doi.org/10.1175/JAM2316.1>.
- Rafieeiniasab, A., Norouzi, A., Kim, S., Habibi, H., Nazari, B., Seo, D.-J., Cosgrove, B., Cui, Z., 2015. Towards high-resolution flash flood prediction in large urban areas — analysis of sensitivity to spatiotemporal resolution of rainfall input and hydrologic modeling. *J. Hydrol.* 531 (2), 370–388. <http://dx.doi.org/10.1016/j.jhydrol.2015.08.045>.
- Ryzhkov, A.V., Zrnic, D.S., 1995. Precipitation and attenuation measurements at a 10-cm wavelength. *J. Appl. Meteorol.* 34 (10), 2121–2134. [http://dx.doi.org/10.1175/1520-0450\(1995\)034<2120:PAAMAA>2.0.CO;2](http://dx.doi.org/10.1175/1520-0450(1995)034<2120:PAAMAA>2.0.CO;2).
- Shakti, P.C., Maki, M., Shimizu, S., Maesaka, T., Kim, D.-S., Lee, D.-I., Iida, H., 2013. Correction of reflectivity in the presence of partial beam blockage over a mountainous region using X-band dual polarization radar. *J. Hydrometeorol.* 14 (3), 744–764. <http://dx.doi.org/10.1175/JHM-D-12-077.1>.
- Trabal, J.M., Colom-Ustariz, J., Cruz-Pol, S., Pablos-Vega, G.A., McLaughlin, D.J., 2013. Remote sensing of weather hazards using a low-cost and minimal infrastructure off-the-grid weather radar network. *IEEE Trans. Geosci. Remote Sens.* 51 (5), 2541–2555. <http://dx.doi.org/10.1109/TGRS.2012.2214227>.
- Turso, S., Zambotto, M., Gabella, M., Orione, F., Notarpietro, R., Perona, G., 2009. Microradarnet: an innovative high-resolution low-cost X-band weather radar network. In: *Proc. Ninth European Conf. on Applications of Meteorology*, Toulouse, France. EMS2009-408 European Meteorological Society.
- van de Beek, C.Z., Leijnse, H., Stricker, J.N.M., Uijlenhoet, R., Russchenberg, H.W.J., 2013. Performance of high-resolution X-band radar for rainfall measurement in The Netherlands. *Hydrol. Earth Syst. Sci.* 14 (2), 205–221. <http://dx.doi.org/10.5194/hess-14-205-2010>.